RSC Advances

PAPER

View Article Online
View Journal | View Issue

Cite this: *RSC Adv.*, 2017, **7**, 18539

A facile fabrication method for ultrathin NiO/Ni nanosheets as a high-performance electrocatalyst for the oxygen evolution reaction†

Yushuai Xu,[a] Kai Huang,[a] Gang Ou,[ab] Hao Tang,[c] Hehe Wei,[a] Qingyun Zhang,[a] Jianghong Gong,[a] Minghao Fang*[c] and Hui Wu*[a]

Received 9th February 2017
Accepted 15th March 2017

DOI: 10.1039/c7ra01683b

rsc.li/rsc-advances

In order to realize the oxygen evolution reaction (OER) with high efficiency on a large scale, a facile method has been created to fabricate NiO/Ni nanosheets by repeated size reduction and thermal oxidation on the surface. By using ultrathin Ni nanosheets with thicknesses of around 4 nm and different temperatures of thermal treatment, tunable oxidation of the metallic nanosheets was achieved. This was proven to have a great impact on the catalysts' electrical conductivity and activity. The NiO/Ni two-dimensional (2D) nano-metal catalyst prepared at 250 °C possesses a potential of 1.59 V (*vs.* RHE) at the current density of 100 mA cm^{-2} in 1 M KOH solution, and still exhibits a high performance after 15 000 cycles. Furthermore, the enhanced electrical conductivity and exposure of active sites contribute to a kinetically low-cost process, resulting in a Tafel slope of 51 mV dec^{-1}. The repeated folding and calendering method is a mature industrial manufacturing procedure, and therefore this creative repeated size reduction and thermal oxidation production process for oxide/metal nanosheets has the potential to be extended to various kinds of metal materials that could be used to produce electrocatalysts in high yields.

Introduction

With the decrease of traditional fossil fuel storage, new kinds of alternative energy resources have been developed.[1,2] Hydrogen, derived from water splitting systems on a large scale,[3,4] has been identified as a kind of renewable high-efficiency energy resource, and promises to replace widely-used fossil energy. However, great challenges still remain when considering the sluggish kinetic rate of the oxygen evolution reaction (OER) process, which is one half of the reaction of water splitting and also a critical step in some other important energy conversion and storage devices, including metal–air batteries[5,6] and fuel cells.[7,8] To achieve a significant improvement in OER, researchers have made great efforts to develop valid electrocatalysts that can greatly enhance this electrochemical process.[9–11] In practice, precious metallic materials, like IrO_2 and RuO_2, in either acidic or alkaline media, are the most commonly used electrocatalysts to drive the oxidation of water and indeed they succeed in this process.[12] However, well-known noble metals with excellent catalytic activity still suffer from high cost and poor reserves, indicating that the anodic oxidation process is currently constrained by limited high performance OER catalysts. Thus, the design of new non-noble metal OER catalysts has drawn extensive attention.

To date a great number of alternatives, including transition metal oxides (NiO, Co_3O_4, MnO_2),[13–15] nitrides (Ni_3N),[16] sulfides (Ni_3S_2),[17] phosphides ($Fe_{10}Co_{40}Ni_{40}P$),[18] mixed transition-metal oxides ($NiCo_2O_4$),[19,20] and layered double hydroxides (LDHs),[21] have been proposed to improve OER catalytic activity. Besides, there is a trend to study carbon-containing or metal-free catalysts, such as MXenes and g-C_3N_4,[22–24] which offer a strategy to lower the cost. With regard to intrinsic activity, first-row transition metals represent a group of the most economic and efficient catalysts, resulting from their unique 3d electron configurations and properties.[18,25] However, most metal oxide electrode materials have failed to exhibit the desirable catalytic activity due to their semiconductor characteristics, essentially suffering from poor electrical conductivity.[26] On the one hand, recent reports have advanced potential solutions from their deep insights into oxide/metal interface nanostructures in liquid phase electrocatalysis, which greatly promote catalytic activity by providing extra active sites and improving the physical properties of metallic substrates.[27,28] The vital role of various kinds of oxide/metal interfaces in different electrochemical reactions has been widely studied, spanning Co/Fe_2O_3, Cu/CeO_2 and Au/Fe_3O_4.[29–31] It is believed that the interfaces contained in these composite nanostructures modify

[a]*State Key Laboratory of New Ceramics and Fine Processing, School of Materials Science and Engineering, Tsinghua University, Beijing 100084, China. E-mail: huiwu@tsinghua.edu.cn*

[b]*Department of Chemistry and Collaborative Innovation Center for Nanomaterial Science and Engineering, Tsinghua University, Beijing 100084, China*

[c]*School of Materials Science and Technology, China University of Geosciences, Beijing, 100083, China. E-mail: fmh@cugb.edu.cn*

† Electronic supplementary information (ESI) available. See DOI: 10.1039/c7ra01683b

electron transport to a great extent and consequently facilitate electrocatalytic processes. On the other hand, to further enhance the activity of unitary metal element based systems, some highly efficient OER catalysts have been constructed from several kinds of metallic elements to stimulate the interconnection between catalytic materials, so providing a superior strategy for catalyst design.[32–34]

Various strategies have been applied to enhance catalytic activity, including constituent and structure design to improve electrical conductivity or electrochemical activity. As is well known to all, nanostructures can offer plenty of active sites. Such structures range from micropowders to nanoparticles (even single atom catalysts) to one-dimensional (1D) nanowires or nanoribbons and two-dimensional (2D) nanosheets; and first row transition metal oxides and their mixed oxides offer better performance than their pure metal counterparts due to their intrinsic activity. Therefore, nanosizing the morphology and diversifying the constituents of electrode materials have become guidelines for catalyst design. In particular, atomic thickness nanosheets have been regarded as one of the most promising materials because of their high surface/volume ratio and amazing electronic properties, since more and more attention has been paid to inorganic graphene analogues with weak van der Waals forces between the layers.[35–37] However, the process of exploring high-efficiency atomic thickness catalysts has shown that the synthetic method is the key to element design, and this is still a bottleneck when considering binary, ternary and multi-element metallic catalysts. Here, we report a facile partial oxidation method for metallic nanosheets based on a scalable, size-controlled metal nanosheet production method combined with subsequent thermal oxidation treatment. When considering the performance of unitary transition metal oxides, NiO exhibits a high OER catalytic activity and low overpotential compared with alternatives, as generally revealed by volcano plots.[2] Besides, due to the availability of Ni materials and their mechanical ductility and catalytic activity, we employ NiO/Ni as a model structure to illustrate our synthesis method for partially oxidized metallic nanosheet OER electrocatalysts in an alkaline environment. The proposed NiO/Ni nanostructures, in which moderate superficial oxidation occurs on the original ultrathin metallic nanosheets after thermal treatment, offer tunable activated NiO sites which accelerate the limited semiconductor charge transfer process for OER.[38]

In this work, NiO/Ni nanosheets are synthesized by repeated folding and calendering (RFC; first reported by our group[39]), in which heterogeneous metallic stacked nanolayers can be achieved from simple Al and Ni foils in the first step (Fig. S1a–c, ESI†). After selective etching, the original Ni nanosheets are available as raw materials (see Experimental section). We note that the as-prepared samples should be stored in a proper environment since ultrathin Ni nanosheets are sensitive to oxygen and water. It must be stated that this fabrication method impacts the surface condition of the NiO/Ni nanosheets to some extent, which means that the natural oxidation of partial metallic nanosheets happens. However, oxides formed during the production process fail to afford a desirable state for electrocatalysis as a result of the instability and non-densification of the oxidized surface layers.[40] Therefore, thermal treatment is used to regulate the surface oxide content and quality, and eventually to contribute to an improvement in catalytic performance.

Experimental section

Preparation of NiO/Ni nanosheets

Ultrathin Ni nanosheets were prepared, following our previous report. In this experiment, Ni foil (purity 99.5%, 0.1 mm in thickness) and Al foil (purity 99.95%, 0.1 mm in thickness) were artificially machined to form an alternant Ni–Al nanolayer structure. The procedure was repeated around 18 times and the Ni–Al bulk was rolled to a stacked foil 0.1 mm thick using a rolling machine. After that, the stacked structure was selectively etched by dilute NaOH, and ultrasonicated to obtain a mixed solution containing Ni nanosheets. Then, to obtain the pure Ni nanosheets, the mixed solution was stewed and rinsed several times with deionized water and ethyl alcohol with the assistance of ultrasonication. After that, purified Ni nanosheets were contained in a porcelain boat and heated in a muffle furnace. Different temperatures (200 °C, 250 °C, 350 °C and 450 °C) were set to seek the optimum conditions for the OER reaction. Heating was maintained for 30 min, and then the NiO/Ni nanosheets were achieved.

Material characterization

Samples for X-ray diffraction (XRD) were stored in ethyl alcohol and then dispersed onto silicon substrates to collect patterns from a D/max-2500 diffraction instrument (Rigaku, Japan) with Cu Kα radiation ($\lambda = 1.54056$). The as-prepared NiO/Ni nanosheets and other contrast samples were observed by field-emission scanning electron microscopy (SEM, MERLIN VP Compact, ZEISS, Germany). The original Ni nanosheet sample was examined by atomic force microscopy (AFM, SPM-9600, SHIMADZU Corporation) in the tapping mode. Transmission electron microscopy (TEM) and high resolution (HR)TEM imaging was conducted on a JEOL-2100 TEM. A Thermo Fisher ESCALAB 250Xi X-ray photoelectron spectrometer (XPS) with Al Kα was used to collect binding energy information on different elements.

Preparation of electrodes

Unless otherwise stated, all the powder catalysts were dispersed onto 1 × 1 cm^2 carbon paper electrodes (Toray Industries, Inc.). NiO/Ni nanosheets or contrast samples (2 mg) were mixed with 750 μL deionized water, 250 μL ethyl alcohol, 30 μL Nafion® 117 solution, and 6 μL *N*,*N*-dimethylformamide (DMF) to form a homogeneous ink, which was then loaded equally onto two pieces of 1 × 1 cm^2 carbon paper, such that each one had a loading of 1 mg cm^{-2}. To assess repeatability, these two electrodes were used for reciprocal verification. The as-prepared carbon electrodes were dried in an oven at 70 °C for 60 min to remove the ethanol, and were then transferred to a vacuum drying oven at 140 °C for another 60 min to evaporate the DMF completely.

Electrochemical measurements

In this work, we conducted the electrochemical tests using a CHI 660E work station with a standard three-electrode system, in an environment of 1 M KOH or 6 M KOH solution. Linear sweep voltammetry (LSV) was performed at a scanning rate of 5 mV s^{-1} employing an Ag/AgCl reference electrode and a Pt mesh counter electrode. Long-term cyclic voltammetry (CV) was performed from 0.2 V to 0.65 V at a scanning speed of 5 mV s^{-1}. All LSV curves were conducted with *iR* compensation and then plotted. AC impedance measurements were carried out in the same system at 0.535 V (*vs.* Ag/AgCl) from 0.01 Hz to 20 kHz.

Results and discussion

The schematic diagram (Fig. 1) shows the procedure used to fabricate scalable size-controlled oxide/metal nanosheets. A large quantity of Ni nanosheets can be achieved through a simple physical size reduction method followed by ultrasound and centrifugation (Fig. S1d, ESI†). To achieve an improvement in catalytic activity, we generated stable NiO on the Ni nanosheets by thermal treatment in an air atmosphere after calendering and purification. An ideal nanostructure consisting of oxides located on ultrathin metallic nanosheets can be obtained. These NiO/Ni nanosheets generally show an expansion of few micrometres following thermal treatment (Fig. 2a and b), but retain their approximate morphology and size after the relatively mild oxidation process, as we can see in the SEM images (Fig. S2a†). As demonstrated in the SEM images (Fig. 2a, b and S2a†), we can also observe that the surfaces of the NiO/Ni nanosheets tend to be rougher than before thermal treatment due to the formation of NiO. From HRTEM images (Fig. 2c, d and S3†), the lattice parameters of the heated nanosheets were identified, and both NiO and Ni can be found on the synthesized nanosheets, as we desired, which confirms the existence of the oxide/metal structure at the scale of an individual nanosheet. Furthermore, AFM (Fig. 2e and f) confirms the thickness of the synthesized NiO/Ni nanosheets at around 3.62 nm. As we know, a general strategy for the production of partially oxidized 2D metal nanosheets for most processable metallic materials is of great importance. Since our fabrication method can be applied to a wide range of metals, including many promising catalytic materials, as proven in our previous paper,[39] all possibilities for the extensive development of 2D functional nanosheets remain open.

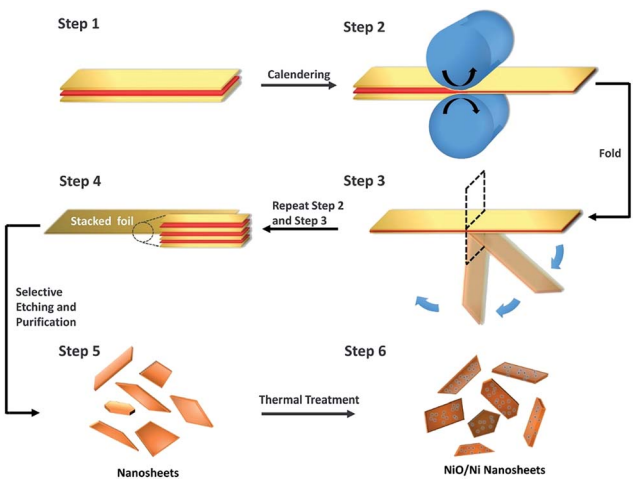

Fig. 1 Procedure of a general partial oxidation fabrication method for 2D metallic electrocatalysts.

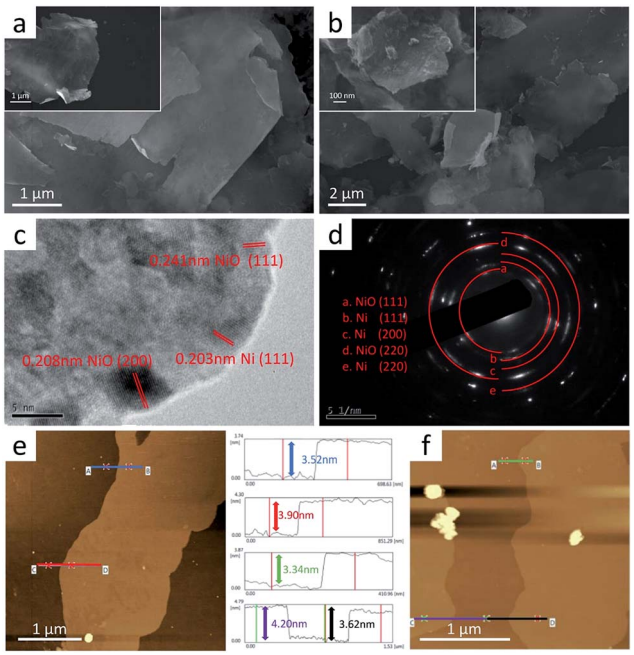

Fig. 2 Morphology illustrations and characterizations of Ni nanosheets before and after thermal treatment: (a) SEM images of Ni nanosheets; (b) SEM images of Ni nanosheets after heating at 250 °C for 30 min; (c) HRTEM images of Ni nanosheets after heating at 250 °C for 30 min; (d) selected-area electron diffraction (SAED) pattern of Ni nanosheets after heating at 250 °C for 30 min; (e) and (f) AFM images of original Ni nanosheets.

The XRD patterns (Fig. 3a) of NiO/Ni nanosheets after thermal treatment at 250 °C (Ni nanosheets-250) and the original nanosheets can be well indexed to JCPDS cards 70-1849 (Ni) and 75-0197 (NiO), which suggests that all the as-prepared samples have the configuration of NiO/Ni. It is clear that surface NiO supported by a metallic Ni substrate can be produced after thermal treatment. Furthermore, XPS analysis was used to demonstrate the elemental compositions, their oxidation states and approximate proportions. Ni and O are the basic elements for the NiO/Ni nanosheets, which can be verified by TEM element mapping (Fig. S4, ESI†) and NiO shows a uniform distribution as well. According to the XPS fitting result of Ni $2p_{3/2}$ (Fig. 3b), four notable peaks are positioned around 852.18 eV, 855.9 eV, 856.6 eV, and 861.17 eV; they can be attributed to Ni^0, Ni^{2+} and satellite peaks, which match well with previous reports.[25,41] From the XPS spectrum of O 1s (Fig. 3c), a great deal of information can be gathered about adsorbed H_2O and oxygen with C, identified around 532.6 eV and 531.8 eV, respectively.[42] These peaks can be attributed to the further oxidation of the samples during storage before the

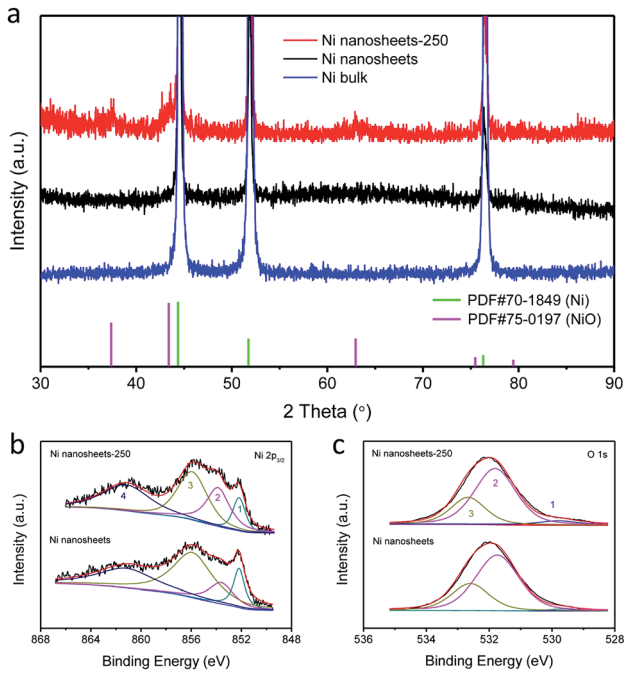

Fig. 3 Structure illustrations of Ni nanosheets, Ni nanosheets thermally treated at 250 °C, and Ni bulk: (a) XRD patterns of NiO/Ni nanosheets prepared in this work; XPS spectra of (b) Ni $2p_{2/3}$; peak 1 refers to Ni^0, peaks 2, 3 refers to Ni^{2+}, peak 4 is a satellite; and (c) O 1s; peaks 1–3 refer to lattice O in NiO, oxygen with C, and adsorbed H_2O, respectively.

XPS test. With the increase of lattice oxygen around 529.8 eV, we further prove the formation of NiO on the Ni nanosheets. With increasing temperature of thermal treatment, there is a trend to a stronger oxidation process (Fig. S5†). Notably, under the same oxidation conditions, the thinner the nanosheets are, the higher the ratio of oxides, which is important for detection of a large amount of NiO. The surface chemical condition of these OER-orientated oxide/metal nanostructures was well explained by XPS, a surface-sensitive detection technique. That is, surface electron transfer, as a fundamental step of electrochemical catalytic processes, can be favoured by these widely-studied metal/oxide nanostructures. To sum up, data from XRD and XPS can prove the co-existence of NiO and Ni on a large scale, which strongly suggests that these nanostructures will be promising OER electrocatalysts.

To realize NiO/Ni nanosheets with tunable OER electrocatalytic activity, counterparts of different sizes and morphologies were selected as the reference catalysts (Fig. S6 and S7†). We analysed the electrocatalytic OER activity of NiO/Ni nanosheets in alkaline solutions (1 M or 6 M KOH) in a standard three-electrode system. Different Ni metallic based catalysts were loaded on carbon paper as working electrodes and then checked for their OER electrocatalytic activity. To investigate the influence of temperature on OER performance, samples prepared at different thermal treatment temperatures were examined, as shown in Fig. S6.† An optimal catalytic activity can be obtained at an intermediate temperature of around 250 °C for 30 min. As shown in the LSV curves, the electrode coated with the NiO/Ni nanosheets-250 sample offers a pretty low potential of 1.59 V (*vs.* RHE) at 100 mA cm^{-2} in 1 M KOH (Fig. 4a). Even in 6 M KOH, the examined catalysts display the same order (Fig. S9†), indicating that a proper annealing temperature is a key factor in this fabrication process. Moreover, an obvious Ni^{2+} to Ni^{3+} oxidation peak from the enlarged plot of the NiO/Ni nanosheets' performance in 6 M KOH (Fig. S8†) confirms the active role of NiO during the OER process.[13]

To better understand the OER kinetics of the different Ni metallic based electrodes, the Tafel slopes shown in Fig. 4b were derived from polarization curves according to the Tafel equation.[2] The NiO/Ni nanosheets-250 sample displays the lowest Tafel slope of 51 mV dec^{-1}, which is among the best of those reported for metallic oxide catalysts. It is believed that the relatively smaller Tafel slope value for the NiO/Ni nanosheets-250 sample can be attributed to its highly conserved conductivity from the Ni nanosheet substrate. To uncover the deeper principles, electrochemical impedance spectroscopy (EIS) measurements were also conducted (Fig. 4d). According to the analysis of EIS, nearly all catalytic materials exhibit a capacitive semicircle and the NiO/Ni nanosheets-250 sample displays the smallest circle when compared with its NiO/Ni nanosheets-350 counterpart and the nanopowders. Since the diameter of the semicircle in EIS spectra indicates the charge transfer resistance, a rapid electron transport can be expected on the surface of the NiO/Ni nanosheets-250 sample because it has the lowest resistance during the OER process. Besides, the *x*-axis intersection represents the solution resistance, partly resulting from interfacial contact resistance and the catalytic materials' intrinsic resistance.[16,43–45] It can be concluded that, with the increase in the extent of oxidation, the solution resistance

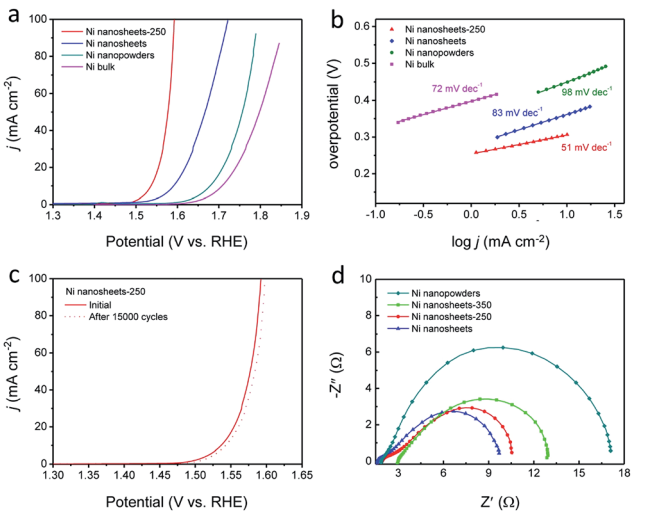

Fig. 4 Electrochemical characterization of prepared Ni nanosheets, Ni thermally treated at 250 or 350 °C and their powders or bulk counterparts for comparison: (a) polarization curves of as-prepared electrode materials in 1 M KOH; (b) Tafel slope plots of the as-mentioned electrode materials; (c) durability measurements of Ni nanosheets thermally treated at 250 °C; and (d) Nyquist plots of materials mentioned in this work.

increases. Therefore, it can be inferred that a moderate level of oxidation for NiO/Ni configurations can not only generate sufficient NiO active sites for OER but can also retain a higher level of electrical conductivity from the ultrathin Ni nanosheet substrate. Another important indicator for a catalyst is its durability, and so long-term CV measurements were made of the NiO/Ni catalyst annealed at 250 °C. Only a slight attenuation of OER current density was observed during 15 000 cycles (Fig. 4c), which strongly suggests the superior stability of this NiO/Ni nanosheet catalyst and indicates its potential practical use.

Conclusions

To sum up, we propose a general mass production strategy for advanced OER electrocatalysts, based on a new synthetic method for 2D partly oxidized metallic nanostructures. As an illustrative material, we prepared partly oxidized NiO/Ni nanosheets by heating at 250 °C for 30 min. These nanosheets display an exceptional potential of 1.59 V (*vs.* RHE) at 100 mA cm^{-2}, and a Tafel slope of 51 mV dec^{-1}. The enhancement of catalytic activity and stability can be attributed to two aspects: on the one hand, the large surface/volume ratio of the Ni nanosheets and the unique electronic properties of the atomic thickness structure (as a result of repeated size reduction together with partial surface oxidation) offer promise for catalytic activity in the OER reaction; on the other hand, a favourable oxide/metal structure is selected by the thermal treatment method, leading to surface oxide stabilization and densification. The mass production of the original metallic nanosheets and the controlled atmospheric thermal oxidation open a new window for the development of oxide/metal advanced electrocatalysts for practical OER applications and other fields concerned with potential energy conversion and storage.

Acknowledgements

This study was supported by the National Basic Research of China (Grants 2015CB932500), the National Natural Science Foundations of China (Grant 51661135025 and 51522207) and the China Postdoctoral Science Foundation (Grant No. 2016M601019). H. Wu acknowledges the support from the 1000 Youth Talents Plan of China.

Notes and references

1 S. Chu and A. Majumdar, *Nature*, 2012, **488**, 294.
2 Y. Jiao, Y. Zheng, M. Jaroniec and S. Z. Qiao, *Chem. Soc. Rev.*, 2015, **44**, 2060.
3 H. T. Wang, H. W. Lee, Y. Deng, Z. Y. Lu, P. C. Hsu, Y. Y. Liu, D. C. Lin and Y. Cui, *Nat. Commun.*, 2015, **6**, 7261.
4 Y. Yang, H. L. Fei, G. D. Ruan and J. M. Tour, *Adv. Mater.*, 2015, **27**, 3175.
5 F. Y. Cheng and J. Chen, *Chem. Soc. Rev.*, 2012, **41**, 2172.
6 H. Y. Ma and B. G. Wang, *RSC Adv.*, 2014, **4**, 46084.
7 W. T. Hong, M. Risch, K. A. Stoerzinger, A. Grimaud, J. Suntivich and Y. Shao-Horn, *Energy Environ. Sci.*, 2015, **8**, 1404.
8 J. W. D. Ng, M. García-Melchor, M. Bajdich, P. Chakthranont, C. Kirk, A. Vojvodic and T. F. Jaramillo, *Nat. Energy*, 2016, **1**, 16053.
9 P. Z. Chen, K. Xu, T. P. Zhou, Y. Tong, J. C. Wu, H. Cheng, X. L. Lu, H. Ding, C. Z. Wu and Y. Xie, *Angew. Chem., Int. Ed.*, 2016, **55**, 2488.
10 F. Dionigi and P. Strasser, *Adv. Energy Mater.*, 2016, **6**, 23.
11 Y. F. Sun, S. Gao, F. C. Lei and Y. Xie, *Chem. Soc. Rev.*, 2015, **44**, 623.
12 X. X. Zou, A. Goswami and T. Asefa, *J. Am. Chem. Soc.*, 2013, **135**, 17242.
13 R. D. L. Smith, M. S. Prévot, R. D. Fagan, Z. P. Zhang, P. A. Sedach, M. K. J. Siu, S. Trudel and C. P. Berlinguette, *Science*, 2013, **340**, 60.
14 Y. Gorlin and T. F. Jaramillo, *J. Am. Chem. Soc.*, 2010, **132**, 13612.
15 Y. F. Sun, S. Gao, F. C. Lei, J. W. Liu, L. Liang and Y. Xie, *Chem. Sci.*, 2014, **5**, 3976.
16 K. Xu, P. Z. Chen, X. L. Li, Y. Tong, H. Ding, X. J. Wu, W. S. Chu, Z. M. Peng, C. Z. Wu and Y. Xie, *J. Am. Chem. Soc.*, 2015, **137**, 4119.
17 W. Zhou, X. J. Wu, X. Cao, X. Huang, C. L. Tan, J. Tian, H. Liu, J. Y. Wang and H. Zhang, *Energy Environ. Sci.*, 2013, **6**, 2921.
18 Z. Zhang, J. H. Hao, W. S. Yang and J. L. Tang, *RSC Adv.*, 2016, **6**, 9647.
19 R. D. L. Smith, M. S. Prévot, R. D. Fagan, S. Trudel and C. P. Berlinguette, *J. Am. Chem. Soc.*, 2013, **135**, 11580.
20 C. Z. Yuan, H. B. Wu, Y. Xie and X. W. Lou, *Angew. Chem., Int. Ed.*, 2014, **53**, 1488.
21 H. F. Liang, F. Meng, M. Cabán-Acevedo, L. S. Li, A. Forticaux, L. C. Xiu, Z. C. Wang and S. Jin, *Nano Lett.*, 2015, **15**, 1421.
22 T. Y. Ma, J. L. Cao, M. Jaroniec and S. Z. Qiao, *Angew. Chem., Int. Ed.*, 2016, **55**, 1138.
23 J. Q. Tian, Q. Liu, A. M. Asiri, K. A. Alamry and X. P. Sun, *ChemSusChem*, 2014, **7**, 2125.
24 J. T. Zhang, Z. H. Zhao, Z. H. Xia and L. M. Dai, *Nat. Nanotechnol.*, 2015, **10**, 444.
25 T. Reier, Z. Pawolek, S. Cherevko, M. Bruns, T. Jones, D. Teschner, S. Sören, B. Arno, H. N. Nong, R. Schlögl, K. J. J. Mayrhofer and P. Strasser, *J. Am. Chem. Soc.*, 2015, **137**, 13031.
26 V. Viswanathan, K. L. Pickrahn, A. C. Luntz, S. F. Bent and J. K. Nørskov, *Nano Lett.*, 2014, **14**, 5853.
27 Z. Weng, W. Liu, L. C. Yin, R. P. Fang, M. Li, E. I. Altman and H. L. Wang, *Nano Lett.*, 2015, **15**, 7704.
28 D. H. Deng, K. S. Novoselov, Q. Fu, N. F. Zheng, Z. Q. Tian and X. H. Bao, *Nat. Nanotechnol.*, 2016, **11**, 218.
29 K. J. McDonald and K. S. Choi, *Chem. Mater.*, 2011, **23**, 1686.
30 X. Q. Wang, J. A. Rodriguez, J. C. Hanson, D. Gamarra, A. Martínez-Arias and M. Fernández-García, *J. Phys. Chem. B*, 2006, **110**, 428.
31 Y. Lee, M. A. Garcia, N. A. Frey Huls and S. Sun, *Angew. Chem., Int. Ed.*, 2010, **122**, 1293.
32 B. Zhang, X. L. Zheng, O. Voznyy, R. Comin, M. Bajdich, M. García-Melchor, L. L. Han, J. X. Xu, M. Liu, L. R. Zheng,

F. P. G. Arquer, C. T. Dinh, F. J. Fan, M. J. Yuan, E. Yassitepe, N. Chen, T. Regier, P. F. Liu, Y. H. Li, P. D. Luna, A. Janmohamed, H. L. Xin, H. G. Yang, A. Vojvodic and E. H. Sargent, *Science*, 2016, **352**, 333.

33 Z. Y. Lu, L. Qian, Y. Tian, Y. P. Li, X. M. Sun and X. Duan, *Chem. Commun.*, 2016, **52**, 908.

34 M. K. Bates, Q. Y. Jia, H. Doan, W. T. Liang and S. Mukerjee, *ACS Catal.*, 2015, **6**, 155.

35 S. H. Bae, J. E. Kim, H. Randriamahazaka, S. Y. Moon, J. Y. Park and I. K. Oh, *Adv. Energy Mater.*, 2017, **7**, 1601492.

36 Y. F. Sun, S. Gao, F. C. Lei, C. Xiao and Y. Xie, *Acc. Chem. Res.*, 2014, **48**, 3.

37 Y. Xiao, L. G. Feng, C. Q. Hu, V. Fateev, C. P. Liu and W. Xing, *RSC Adv.*, 2015, **5**, 61900.

38 Y. Kuang, G. Feng, P. S. Li, Y. M. Bi, Y. P. Li and X. M. Sun, *Angew. Chem., Int. Ed.*, 2016, **55**, 693.

39 H. W. Liu, H. Tang, M. H. Fang, W. J. Si, Q. H. Zhang, Z. H. Huang, L. Gu, W. Pan, J. Yao, C. W. Nan and H. Wu, *Adv. Mater.*, 2016, **28**, 8170.

40 E. S. Lambers, C. N. Dykstal, J. M. Seo, J. E. Rowe and P. H. Holloway, *Oxid. Met.*, 1996, **45**, 301.

41 X. D. Yan, L. Tian and X. B. Chen, *J. Power Sources*, 2015, **300**, 336.

42 A. N. Mansour, *Surf. Sci. Spectra*, 1994, **3**, 231.

43 X. Long, Z. J. Ma, H. Yu, X. Y. Gao, X. Y. Pan, X. X. Chen, S. H. Yang and Z. G. Yi, *J. Mater. Chem. A*, 2016, **4**, 14939.

44 C. Z. Yuan, J. Y. Li, L. R. Hou, J. D. Lin, X. G. Zhang and S. L. Xiong, *J. Mater. Chem. A*, 2013, **1**, 11145.

45 G. F. Zeng, M. Liao, C. X. Zhou, X. J. Chen, Y. J. Wang and D. Xiao, *RSC Adv.*, 2016, **6**, 42255.

